Indian Journal of Chemistry
Vol. 47A, February 2008, pp. 186-193

Palladium catalysts doped in $Ce_xZr_{1-x}O_2$ washcoated monoliths for toluene combustion

Qingbao Zhang, Leihong Zhao*, Botao Teng, Mengfei Luo, Yunlong Xie & Lei Yue

Zhejiang Key Laboratory for Reactive Chemistry on Solid Surfaces, Institute of Physical Chemistry, Zhejiang Normal University, Jinhua 321004, PR China

Email: zhaoleihong@163.com

Received 20 July 2007; revised 24 December 2007

A novel $Ce_xZr_{1-x}O_2$ washcoat has been prepared by an impregnation method, which acts as a host for the active Pd component to prepare a series of the Pd-$Ce_xZr_{1-x}O_2$/monolith (x=1, 0.8, 0.6 and 0.5) catalysts for toluene combustion. SEM, BET, XRD, Raman spectroscopy, and H_2-TPR techniques have been used to characterize the samples. The washcoat shows excellent adhesion to the monolith. The Zr component of the Pd-$Ce_xZr_{1-x}O_2$/monolith catalysts plays an important role in the catalytic activity for toluene combustion and the order of the catalytic activity is $x = 0.8>0.6>0.5\approx1$. There is strong interaction among palladium, ceria-zirconia solid solution and the monolith.

IPC Code: Int. Cl.[8] B01J21/00; B01J37/00

Monolithic catalyst supports can be an attractive replacement for conventional carriers in heterogeneous catalysts and are widely applied to the purification of automotive exhaust gases, the catalytic combustion of methane, and the elimination of volatile organic compounds (VOCs)[1-3]. The most common material for the monolithic support is cordierite monolith due to low pressure drop, low thermal expansion coefficient, high mechanical strength and high thermal shock resistance[1,4]. For practical applications, the monolithic support is usually pre-coated by a γ-alumina washcoat with high surface area. Nevertheless, γ-alumina transforms into α-alumina with low surface area at high temperature resulting in the catalytic activity degradation[5,6]. Accordingly, the promoters, such as CeO_2, La_2O_3, and BaO[6-8], have been generally used to inhibit the phase transformation and enhance the catalytic activity. However, when calcined at high temperature, the spinel formation occurs due to the reaction between γ-alumina and the promoters leading to the destruction of the active species. Furthermore, another important disadvantage of γ-alumina washcoat is the formation of the deep creeps due to the different thermal dilation coefficient between the cordierite monolith and the active phase[9]. Therefore, the development of new valid washcoat materials is eagerly desired.

One of the very promising washcoat materials are ceria-based oxides, especially noble metal loaded CeO_2-ZrO_2 mixed oxides due to their excellent oxygen storage capacity, high thermal stability, enhanced redox and catalytic properties[10-15]. Therefore, ceria-zirconia mixed oxides are currently regarded as potentially practical materials used as support or main component in the washcoat in the third generation of three-way catalysts (TWCs)[16,17]. On the other hand, supported palladium catalysts have potential industrial applications in the total combustion of hydrocarbons due to their cheaper price compared with other noble metals in the market, excellent oxidation activity[18], and high temperature durability[19]. Although Pd-loaded CeO_2-ZrO_2 mixed oxides have been used as TWCs, research on the catalysts has been focused on the enhancement of oxygen storage capacity and the improvement of their thermal stability. There has been little attention to ceria-zirconia mixed oxides used as the washcoat materials. This prompted us to carry out the present investigations.

The new $Ce_xZr_{1-x}O_2$ washcoat reported herein, has been used as the washcoat of the Pd-$Ce_xZr_{1-x}O_2$/monolith (x=1, 0.8, 0.6 and 0.5) catalysts. The adhesion of the washcoat was evaluated using an ultrasonic technique. The surface morphology, the structure, the catalytic activity for toluene combustion and the redox behavior of the catalysts were also investigated.

Materials and Methods

A commercial cordierite monolith ($2MgO{\cdot}2Al_2O_3{\cdot}5SiO_2$, in form of 48×24×40 mm^3 cuboid) was used. The monolith had square channels, a cell density of 200 cpsi (cells per square inch), and a wall thickness of approximate 0.33 mm. The catalysts were prepared as follows: A mixture of $Ce(NO_3)_3{\cdot}6H_2O$ and $Zr(NO_3)_4{\cdot}5H_2O$ with a molar ratio of Ce:Zr=x:1-x (x=1, 0.8, 0.6 and 0.5) was dissolved into distilled water. The citric acid monohydrate was used as complexing agent in 1.5:1 molar ratio with respect to the sum of metal salts. The solution heated at 80°C in a water bath was constantly stirred. Appropriate amounts of 95% ethanol and polyethylene glycol (PEG) with an average molecular weight of 10000 were added as dispersant and binder, respectively. Then, an appropriate amount of aqueous solution of H_2PdCl_4 was added. The washcoating was carried out by dipping of the cordierite monolith in the solution. The washcoated monolith was blown with air to remove the excessive solution. It was dried at room temperature overnight in air, and then at 130°C for 4 h in an oven, followed with calcination at 400°C for 1 h under a static air in a muffle furnace. The dipping and drying procedure was repeated, and then the catalysts were calcined at 400°C for 2 h. The nominal mass percentage of Pd was 0.1% and $Ce_xZr_{1-x}O_2$ mixed oxides was 6%, respectively. The catalyst obtained was designed as Pd-$Ce_xZr_{1-x}O_2$/monolith. $Ce_xZr_{1-x}O_2$ (x=1, 0.8, 0.6 and 0.5) powder samples were prepared similarly except that the aqueous solution of H_2PdCl_4 and the washcoating were not performed, while Pd-$Ce_xZr_{1-x}O_2$ (x=1, 0.8, 0.6 and 0.5) powder samples were prepared following similar procedure except that the washcoating was not carried out.

The sample morphology was examined with a Hitachi S-4800 scanning electron microscopy (SEM) operated at an accelerated voltage of 15 kV. The samples were glued to the sample holder with silver paint and sputtered with gold to make them more conductive. The ultrasonic test was performed in order to evaluate the cohesive ability of the washcoat. The samples were subjected to ultrasound by immersing them in water inside a glass vessel and in an ultrasonic bath (KU-200 ultrasonic vibration cleaner, 40 kHz and 220 W) for 60 min. After that, the samples were dried and weighed. The weight loss was calculated as follows:

$$\Delta W(\%) = \frac{W_{before} - W_{after}}{W_{before}} \times 100$$

where W_{before} and W_{after} are the washcoat weight before and after the ultrasonic treatment, respectively. Brunauner-Emmett-Teller (BET) surface area was determined by N_2 adsorption at 77 K using a Quantachrome Autosorb-1 apparatus.

X-ray powder diffraction (XRD) patterns were recorded with a Philips PW3040/60 powder diffractometer, operated at 40 kV and 40 mA, using nickel-filtered CuK_α (λ=0.1542 nm) radiation. The Raman spectra were obtained on a Renishaw RM1000 confocal microscope. The 514.5 nm line of an argon ion laser was used and the laser power at the sample was set at 3 mW.

Hydrogen temperature-programmed reduction (H_2-TPR) measurement was carried out in a quartz microreactor. About 100 mg (or 25 mg for the powder sample) sample was used in each measurement. After introducing the reduction agent of H_2-N_2 (5-95%) with a total flow rate of 20 $mL{\cdot}min^{-1}$, the sample was heated from room temperature to 860°C with a heating rate 10°C min^{-1}. The amount of H_2 uptake during reduction was measured by a thermal conductivity detector (TCD), which was calibrated by the quantitative reduction of CuO to the metallic copper.

Catalytic activity

The as-prepared Pd-$Ce_xZr_{1-x}O_2$/monolith catalyst was cut into two cylinders (length=40 mm, i.d.=21 mm) for the catalytic activity test. The catalytic combustion of toluene over the Pd-$Ce_xZr_{1-x}O_2$/monolith catalyst was carried out in a fixed bed reactor with an inner diameter of 22 mm and a length of 600 mm. The concentration of toluene in air was 40000 $mg{\cdot}m^{-3}$ and the total flow rate was 0.3 m^3 h^{-1} corresponding to a gas hourly space velocity (GHSV) of 10800 h^{-1}. The concentration of toluene was analyzed by a GC-14C (Shimadzu) equipped with Supelcowax 10 column (30 m × 0.25 mm × 0.25 μm) and an FID detector. In typical runs, the reaction data were obtained after the catalytic combustion of toluene was performed more than 30 min in order to achieve the steady state. No other carbon containing compounds except CO_2 in the products were detected during the activity test. Thus, toluene conversion was calculated as:

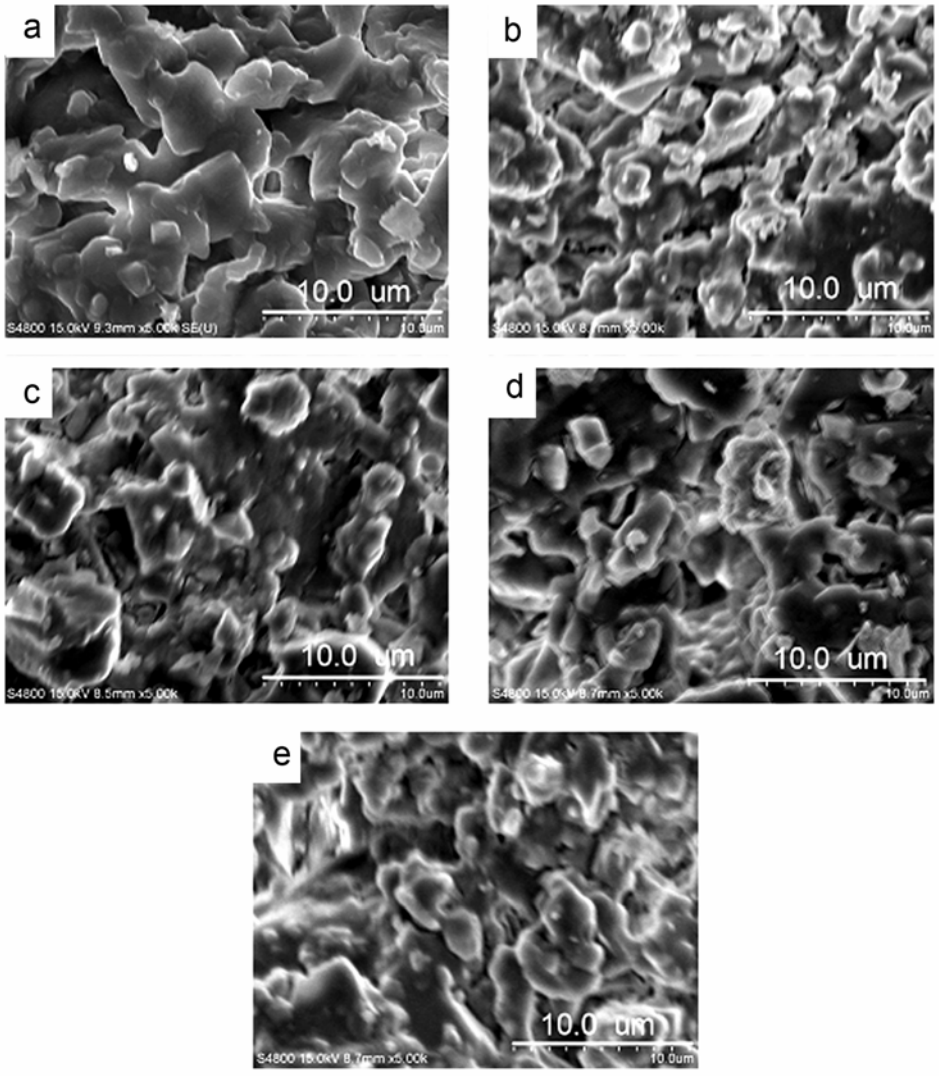

Fig. 1 — SEM micrographs of the bare monolith and the Pd-$Ce_xZr_{1-x}O_2$/monolith catalysts (top view of the channels with magnification 5000) [(a) the bare monolith; (b) the Pd-CeO_2/monolith catalyst; (c) the Pd-$Ce_{0.8}Zr_{0.2}O_2$/monolith catalyst; (d) the Pd-$Ce_{0.6}Zr_{0.4}O_2$/monolith catalyst; and (e) the Pd-$Ce_{0.5}Zr_{0.5}O_2$/monolith catalyst].

$$\text{Toluene conversion}(\%) = \frac{[\text{toluene}]_{in} - [\text{toluene}]_{out}}{[\text{toluene}]_{in}} \times 100$$

where $[\text{toluene}]_{out}$ is the toluene concentration in the products, and $[\text{toluene}]_{in}$ is the toluene concentration of the feed gas.

Results and Discussion

The surface morphology of the bare monolith and the Pd-$Ce_xZr_{1-x}O_2$/monolith (x=1, 0.8, 0.6 and 0.5) catalysts can be compared in the SEM micrographs as shown in Fig. 1. It has been found that the Pd-$Ce_xZr_{1-x}O_2$/monolith catalysts do not show a visible boundary, implying that the washcoat tightly inosculates with the monolith. This might be ascribed to the fact that CeO_2 and ZrO_2 are both the ceramic materials and they easily interlock with the cordierite monolith. Therefore, the interaction between the washcoat and the monolith may be quite strong, and the washcoat might tightly anchor onto the monolith, which will be further verified by an ultrasonic test. In addition, it appears that the surface morphology of all catalysts at a magnification of 5000 times is similar and does not depend on the molar ratio of Ce to Zr in the catalysts.

In order to further validate the cohesive ability of the washcoat of the catalyst, an ultrasonic test was employed as a severe method of adherance testing[1] to evaluate the washcoat adherence, and the corresponding results are listed in Table 1. The weight losses of all the Pd-$Ce_xZr_{1-x}O_2$/monolith catalysts are less than or equal to 3.0%, indicating that all the washcoats show excellent adhesion to the monoliths.

As listed in Table 2, the surface area of the monolith is only 0.5 m^2g^{-1}, while those of the Pd-$Ce_xZr_{1-x}O_2$/monolith catalysts are similar, i.e. 4.8 m^2g^{-1}, 4.7 m^2g^{-1}, 4.4 m^2g^{-1}, 4.1 m^2g^{-1}, which corresponds to x from 1 to 0.5, respectively. This might be attributed to the comparable surface morphology of the catalysts.

Since the low content of the $Ce_xZr_{1-x}O_2$ mixed oxides (6 wt. %.) and the Pd (0.1 wt. %) and limited XRD sensitivity, the peaks of the cordierite monolith cover the characteristic peaks of the $Ce_xZr_{1-x}O_2$ mixed oxides and the Pd. As a result, the available information is little. Accordingly, the XRD patterns of the corresponding powder samples without monoliths were carried out as illustrated in Fig. 2. It has been found that all the diffraction peaks of the powder samples can be indexed to (111), (200), (220) and (311) crystal planes, corresponding to the cubic fluorite structure of CeO_2. This is an indication that ZrO_2 could be incorporated into the CeO_2 lattice to form a ceria-zirconia solid solution while maintaining the fluorite structure, which is in agreement with the reported results[20-22]. In addition, there is a small but continuous shift of the XRD peaks to higher 2θ values with an increase in Zr content, which is ascribed to the replacement of Ce^{4+} (0.97 Å) with a smaller cationic radius Zr^{4+} (0.84 Å) resulting in the shrinkage of lattice.

In order to further obtain the information of the phase, the Raman experiments were carried out and the corresponding results are presented in Fig. 3. Figure 3a shows that there is one strong absorption peak centered at about 465 cm^{-1} for the catalysts, which is typical of the F_{2g} Raman active mode of the cubic fluorite structure of CeO_2[23]. With a decrease in x (from 1 to 0.5), the intensity of CeO_2 absorption peak strongly weakens, which is reported already[24,25]. In addition, the spectra exhibit the Raman line at 650 cm^{-1} associated with the Raman active B_{1g} vibrational mode of PdO[26]. As for the corresponding powder samples (Fig. 3b), the spectra also exhibit the characteristic absorption peaks of CeO_2 and PdO. No peaks associated with free ZrO_2 are present, which further confirms the formation of ceria-zirconia solid solution in the powder samples, as showed in the

Table 1 — Weight losses of the Pd-$Ce_xZr_{1-x}O_2$/monolith catalysts treated by ultrasonic vibration

Sample	ΔW (%)
Pd-CeO_2/monolith	1.1
Pd-$Ce_{0.8}Zr_{0.2}O_2$/monolith	1.2
Pd-$Ce_{0.6}Zr_{0.4}O_2$/monolith	2.1
Pd-$Ce_{0.5}Zr_{0.5}O_2$/monolith	3.0

Table 2 — BET surface areas of the Pd-$Ce_xZr_{1-x}O_2$/monolith catalysts, the monolith, the Pd-$Ce_xZr_{1-x}O_2$ powder samples and the $Ce_xZr_{1-x}O_2$ powder samples

Sample	BET surface area (m^2g^{-1})
Pd-CeO_2/monolith	4.8[a]
Pd-$Ce_{0.8}Zr_{0.2}O_2$/monolith	4.7[a]
Pd-$Ce_{0.6}Zr_{0.4}O_2$/monolith	4.4[a]
Pd-$Ce_{0.5}Zr_{0.5}O_2$/monolith	4.1[a]
Cordierite monolith	0.5
Pd-CeO_2	44.2
Pd-$Ce_{0.8}Zr_{0.2}O_2$	43.3
Pd-$Ce_{0.6}Zr_{0.4}O_2$	40.1
Pd-$Ce_{0.5}Zr_{0.5}O_2$	38.5
CeO_2	50.8
$Ce_{0.8}Zr_{0.2}O_2$	49.0
$Ce_{0.6}Zr_{0.4}O_2$	45.6
$Ce_{0.5}Zr_{0.5}O_2$	41.7

[a]Relative to the total weight (monolith + washcoat)

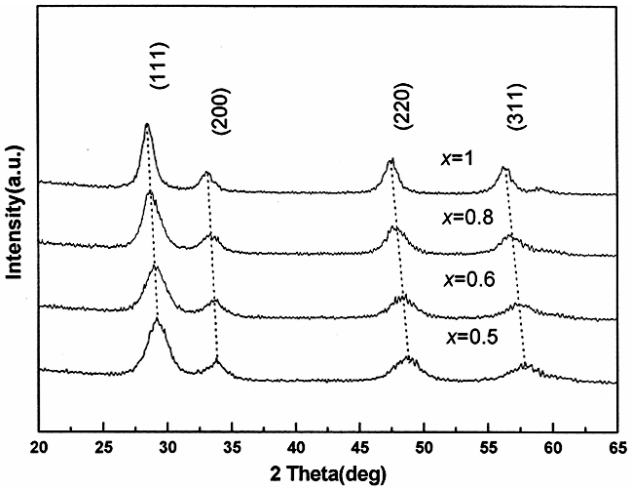

Fig. 2 — XRD patterns of the Pd-$Ce_xZr_{1-x}O_2$ powder samples.

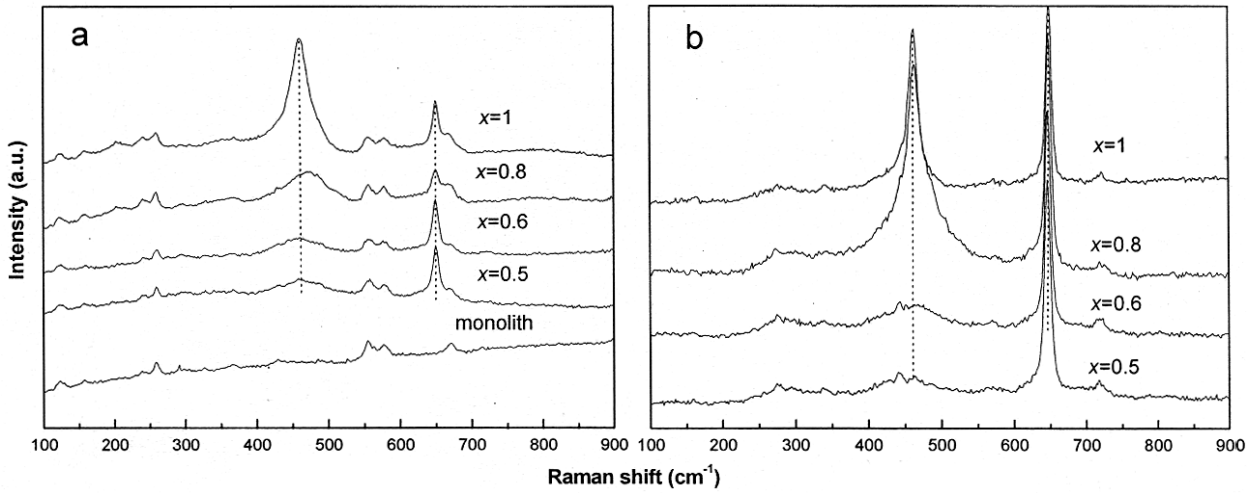

Fig. 3 — Laser Raman spectra of the catalysts, the monolith and the powder samples. [(a) the Pd-$Ce_xZr_{1-x}O_2$/monolith catalysts and the monolith; and (b) the Pd-$Ce_xZr_{1-x}O_2$ powder samples].

XRD analysis. It is obviously found that they exhibit the similar features in comparison with their Laser Raman spectra (Figs 3a and 3b). According to the XRD and Laser Raman analyses above and the results already reported[20-22], it is concluded that the $Ce_xZr_{1-x}O_2$ mixed oxides in the Pd-$Ce_xZr_{1-x}O_2$/monolith catalysts form ceria-zirconia solid solution.

The catalytic combustion of toluene over the Pd-$Ce_xZr_{1-x}O_2$/monolith catalysts is shown in Fig. 4. It has been found that the observed products were carbon dioxide and water in the catalytic combustion of toluene, indicating that complete combustion occurs in the reaction. Figure 4 shows that the catalytic activity of the catalysts depends on the molar ratio of Ce to Zr in the catalysts. The Pd-$Ce_{0.8}Zr_{0.2}O_2$/monolith catalyst exhibits the highest catalytic activity for toluene combustion, over which toluene conversion is up to 98% at 210°C. However, the Pd-$Ce_xZr_{1-x}O_2$/monolith catalysts with x=1 and 0.5 show the lowest catalytic activity. Thus, the order of the catalytic activity in terms of x is 0.8>0.6>0.5≈1, suggesting that the molar ratio of Ce to Zr in the catalysts plays an important role in the catalytic activity for toluene combustion. Therefore, a suitable molar ratio of Ce to Zr in the Pd-$Ce_xZr_{1-x}O_2$/monolith catalysts may be beneficial for the PdO active species.

In order to understand better the catalytic activity performance, the H_2-TPR measurements of the $Ce_xZr_{1-x}O_2$ powder samples, the Pd-$Ce_xZr_{1-x}O_2$ powder samples, the Pd-$Ce_xZr_{1-x}O_2$/monolith catalysts and the monolith were carried out and the results are shown in Fig. 5. Figure 5a shows that the redox properties of the $Ce_xZr_{1-x}O_2$ powder samples are influenced by the molar ratio of Ce to Zr in ceria-zirconia solid solution. The H_2-TPR profile of pure CeO_2 (x=1, the surface area is 50.8 m^2g^{-1} as listed in Table 2) shows two reduction peaks at 514 and 805°C, which is attributed to the reduction of surface and bulk oxygen[13,27], respectively. In addition, the small reduction shoulders at low temperature are ascribed to O^{2-} ions located at various low coordination sites on the oxide crystallites[13]. On the other hand, the surface areas of ceria-zirconia solid

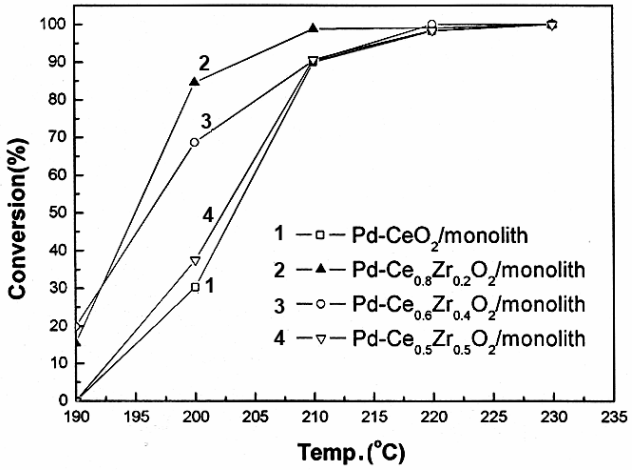

Fig. 4 — Catalytic combustion of toluene over the Pd-$Ce_xZr_{1-x}O_2$/monolith catalysts.

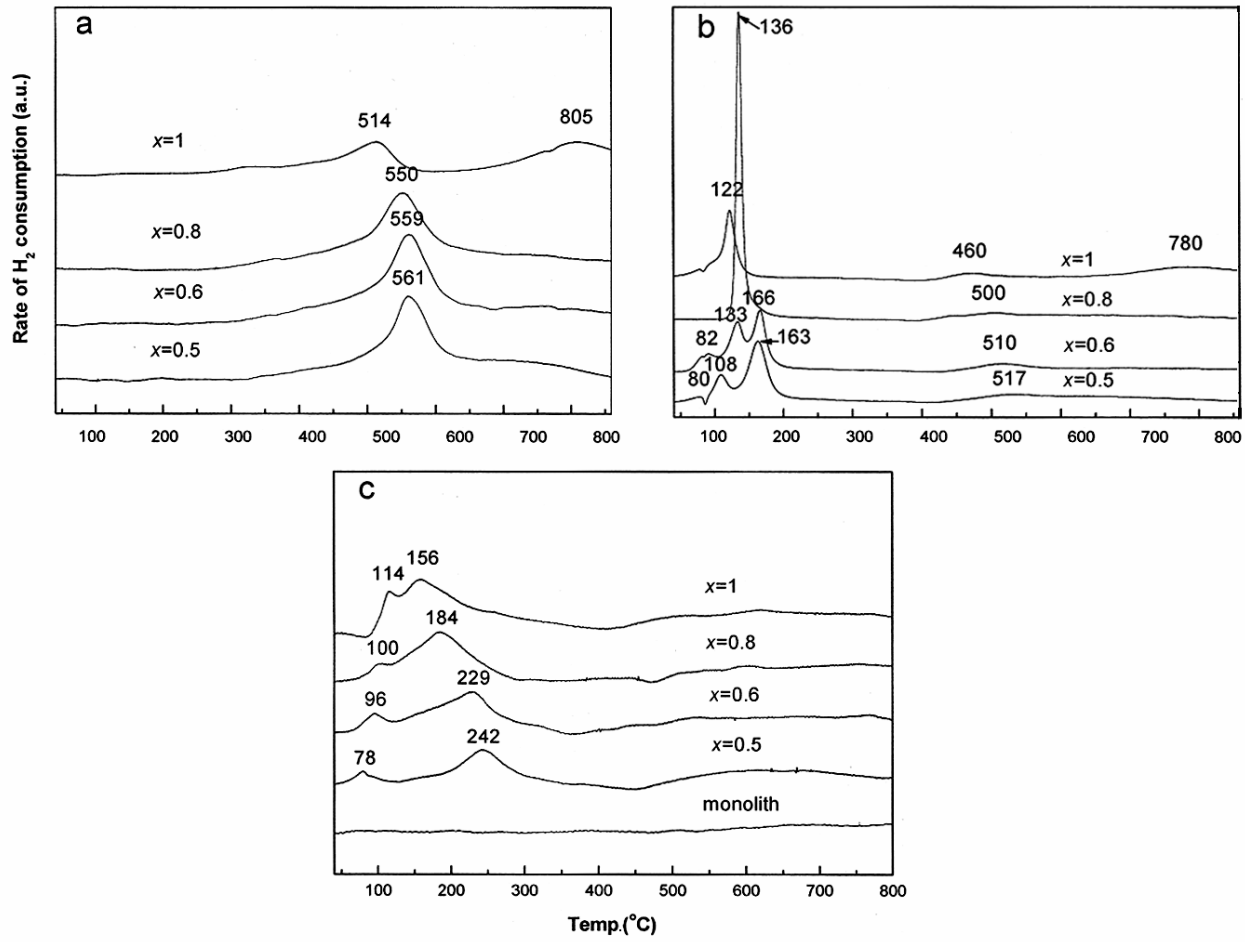

Fig. 5 — H_2-TPR profiles of the powder samples, the catalysts and the monolith [(a) the $Ce_xZr_{1-x}O_2$ powder samples; (b) the Pd-$Ce_xZr_{1-x}O_2$ powder samples; and (c) the Pd-$Ce_xZr_{1-x}O_2$/monolith catalysts and the monolith].

solution (x=0.8, 0.6 and 0.5) are 49.0 m^2g^{-1}, 45.6 m^2g^{-1}, 41.7 m^2g^{-1} (Table 2), respectively. The H_2-TPR profiles of ceria-zirconia solid solution show a main broad peak centered at 550-561°C, suggesting that the reduction of surface and bulk oxygen occurs simultaneously due to increased oxygen mobility in the solid solution[13]. The reduction peak shifts towards higher temperature as Zr content increases, in agreement with the literature[27,28]. The small reduction shoulders are also observed, which is associated with the initial reduction process of the surface oxygen[13]. Thus, the amounts of Zr component in ceria-zirconia solid solution affect the redox properties of the $Ce_xZr_{1-x}O_2$ powder samples.

Figure 5b shows the H_2-TPR profiles of the Pd-$Ce_xZr_{1-x}O_2$ (x=1, 0.8, 0.6 and 0.5) powder samples. It is obviously found that the redox properties of the powder samples are significantly modified when palladium is doped in ceria-zirconia solid solution. The surface areas of the Pd-$Ce_xZr_{1-x}O_2$ (x=1, 0.8, 0.6 and 0.5) powder samples are 44.2 m^2g^{-1}, 43.3 m^2g^{-1}, 40.1 m^2g^{-1}, 38.5 m^2g^{-1} (Table 2), respectively. Pd-CeO_2 (x=1) shows a narrow reduction peak at 122°C, and two weak reduction peaks at 460 and 780°C. The presence of noble metals facilitates the adsorption and spillover of hydrogen from the noble metals particles to the ceria interface, resulting in the ceria reduction at low temperature[13,29]. Therefore, the peak at 122°C may be ascribed to the concurrent reduction of PdO and ceria promoted by noble metal. The two weak peaks at 460 and 780°C are associated with the further reduction of Ce^{4+} species and the reduction of bulk oxygen[13,27,30,31], respectively. Pd-$Ce_{0.8}Zr_{0.2}O_2$ (x=0.8) shows a sharp reduction peak at 136°C and a weak

reduction peak at 500°C assigned to the concurrent reduction of PdO and ceria promoted by noble metal, and the further reduction of Ce^{4+} species, respectively. The peaks both shift towards the higher temperature in comparison with Pd-CeO_2. Pd-$Ce_{0.6}Zr_{0.4}O_2$ (x=0.6) shows three reduction peaks at 82°C, 133°C and 166°C besides a weak reduction peak at 510°C assigned to the further reduction of Ce^{4+} species. The peaks at 82°C and 133°C might be attributed to the reduction of PdO[10,32, 33]. The peak at 166°C might be owned to the reduction of ceria promoted by noble metal. The H_2-TPR profile of Pd-$Ce_{0.5}Zr_{0.5}O_2$ (x=0.5) shows the similar characteristics to that of Pd-$Ce_{0.6}Zr_{0.4}O_2$. However, the former three peaks shift to the lower temperature, while the latter weak peak shifts to the higher temperature in comparison with Pd-$Ce_{0.6}Zr_{0.4}O_2$. The H_2-TPR results indicate that both palladium and the solid solution itself influence the redox properties of the Pd-$Ce_xZr_{1-x}O_2$ powder samples when palladium is doped in the solid solution, and there is the interaction between palladium and ceria-zirconia solid solution, which changes the redox properties of the samples.

Figure 5c shows the H_2-TPR profiles of the Pd-$Ce_xZr_{1-x}O_2$/monolith (x=1, 0.8, 0.6 and 0.5) catalysts and the monolith. It is apparently found that the redox properties of the catalysts are strongly affected when the Pd-$Ce_xZr_{1-x}O_2$ are supported on the monolith. The surface areas of the Pd-$Ce_xZr_{1-x}O_2$/monolith (x = 1, 0.8, 0.6 and 0.5) catalysts are 4.8 m^2g^{-1}, 4.7 m^2g^{-1}, 4.4 m^2g^{-1}, 4.1 m^2g^{-1} (Table 2), respectively. The H_2-TPR profile of the Pd-CeO_2/monolith catalyst shows two reduction peaks at 114 and 156°C. The former peak might be attributed to the reduction of PdO, while the latter peak might be owned to the reduction of ceria promoted by noble metal. With a decrease in x (from 0.8 to 0.5), the former peak shifts to the lower temperature, whereas the latter peak shifts to the higher temperature. It is indicated that the monolith as well as palladium and the solid solution influence the redox properties of the Pd-$Ce_xZr_{1-x}O_2$/monolith catalysts when the Pd-$Ce_xZr_{1-x}O_2$ are supported on the monolith. According to the H_2-TPR results of the $Ce_xZr_{1-x}O_2$ powder samples, the Pd-$Ce_xZr_{1-x}O_2$ powder samples, the Pd-$Ce_xZr_{1-x}O_2$/monolith catalysts and the monolith, it is indicated that there is strong interaction among palladium, ceria-zirconia solid solution and the monolith. The interaction changes the redox properties and influences the catalytic activity of the catalysts.

Conclusions

The Pd-$Ce_xZr_{1-x}O_2$/monolith catalysts have been prepared with $Ce_xZr_{1-x}O_2$ as the novel washcoat. The washcoat shows excellent adhesion to the monolith. The catalytic activity depends on x, and the order of the activity in terms of x is 0.8>0.6>0.5≈1. The Pd-$Ce_{0.8}Zr_{0.2}O_2$/monolith catalyst exhibits the highest catalytic activity for toluene combustion. There is strong interaction among palladium, ceria-zirconia solid solution and the monolith. The interaction changes the redox property and influences the catalytic activity of the catalysts.

Acknowledgement

Natural Science Foundation of China (Grant No.20473075) and Zhejiang Provincial Nature Science Foundation of China (Grant No.203147) are gratefully acknowledged for financial support.

References

1 Nijhuis T A, Beers A E W, Vergunst T, Hoek I, Kapteijn F & Moulijin J A, *Catal Rev*, 43 (2001) 345.

2 Fabbrini L, Rossetti I & Forni L, *Appl Catal B*, 63 (2006) 131.

3 Pérez-Cadenas A F, Kapteijin F, Moulijin J A, Maldonado-Hódar F J, Carrasco-Marín F & Moreno-Castilla C, *Carbon*, 44 (2006) 2463.

4 Geus J W & van Giezen J C, *Catal Today*, 47 (1999) 169.

5 Tijburg I I M, Bruin H De, Elberse P A & Geus J W, *J Mater Sci*, 26 (1991) 5945.

6 Labalme V, Garbowski E, Guihaume N & Primet M, *Appl Catal A*, 138 (1996) 93.

7 Thevenin P O, Alcalde A, Pettersson L J, Järås S G & Fierro J L G, *J Catal*, 215 (2003) 78.

8 Zwinkels M F M, Haussner O, Govind Menon P & Järås S G, *Catal Today*, 47 (1999) 73.

9 Fabbrini L, Rossetti I & Forni L, *Appl Catal B*, 44 (2003) 107.

10 Fornasiero P, Di Monte R, Ranga Rao G, Kašpar J, Meriani S, Trovarelli A & Graziani M, *J Catal*, 151 (1995) 168.

11 Ranga Rao G, Fornasiero P, Di Monte R, Kašpar J, Vlatic G, Balducci G, Meriani S, Gubitosa G, Cremona A & Graziani M, *J Catal*, 162 (1996) 1.

12 Fornasiero P, Ranga Rao G, Kašpar J, L'Erario F & Graziani M, *J Catal*, 175 (1998) 269.

13 Ranga Rao G, *Bull Mater Sci*, 22 (1999) 89.

14 Ranga Rao G, Kašpar J, Fornasiero P, Meriani S, Di Monte R & Graziani M, *Catal Lett*, 24 (1994) 107.

15 Trovarelli A, *Catal Rev-Sci Eng*, 38 (1996) 439.

16 Ozawa M, *J Alloy Compd*, 275-277 (1998) 886.

17 Fernández-García M, Martínez-Arias A, Iglesias-Juez A, Hungría A B, Anderson J A, Conesa J C & Soria J, *Appl*

Catal B, 31 (2001) 39.

18 González-velasco J R, Aranzabal A, Gutiérrez-Ortiz J I, López-Fonseca R & Gutiérrez-Ortiz M A, *Appl Catal B*, 19 (1998) 189.

19 Beck D D & Sommers J W, *Appl Catal B*, 6 (1995) 185.

20 Ranga Rao G & Hanjan Sahu H, *Proc Indian Acad Sci (Chem Sci)*, 113 (2001) 651.

21 Escribano V S, López E F, Panizza M, Resini C, Amores J M G & Busca G, *Solid State Sci*, 5 (2003) 1369.

22 Yu J C, Zhang L Z & Lin J, *J Colloid Interf Sci*, 260 (2003) 240.

23 Fernández-García M, Martínez-Arias A, Iglesias-Juez A, Belver C, Hungría A B, Conesa J C & Soria J, *J Catal*, 194 (2000) 385.

24 Serrano-Ruiz J C, Luettich J, Sepúlveda-Escribano A & Rodríguez-Reinoso F, *J Catal*, 241 (2006) 45.

25 Pokrovski K A & Bell A T, *J Catal*, 241 (2006) 276.

26 McBride J R, Hass K C & Weber W H, *Phys Rev B*, 44 (1991) 5016.

27 Passos F B, de Oliveira E R, Mattos L V & Noronha F B, *Catal Today*, 101 (2005) 23.

28 Ayastuy J L, González-Marcos M P, Gil-Rodríguez A, González-Velasco J R & Gutiérrez-Ortiz M A, *Catal Today*, 116 (2006) 391.

29 He H, Dai H X, Ng L H, Wong K W & Au C T, *J Catal*, 206 (2002) 1.

30 Liotta L F, Macaluso A, Arena G E, Livi M, Centi G & Deganello G, *Catal Today*, 75 (2002) 439.

31 Luo M F, He M, Xie Y L, Fang P & Jin L Y, *Appl Catal B*, 69 (2006) 213.

32 Luo M F & Zheng X M, *Appl Catal A*, 189 (1999) 15.

33 Jen H W, Graham G W, Chun W, McCabe R W, Cuif J P, Deutsch S E & Touret O, *Catal Today*, 50 (1999) 309.